RSC Advances

PAPER

View Article Online
View Journal | View Issue

Cite this: *RSC Adv.*, 2015, **5**, 52533

Controlled synthesis and luminescent properties of assembled spherical $YP_xV_{1-x}O_4:Ln^{3+}$ (Ln = Eu, Sm, Dy or Tm) phosphors with high quantum efficiency

Zhibin An,[a] Xiuzhen Xiao,*[a] Jun Yu,[a] Dongsen Mao[a] and Guanzhong Lu*[ab]

Received 14th May 2015
Accepted 5th June 2015

DOI: 10.1039/c5ra08993j

www.rsc.org/advances

$YP_xV_{1-x}O_4$ (x = 0.3–0.9) assembled spheres with tetragonal phase were prepared hydrothermally under a simple and mild method with the assistance of EDTA. The structures and shapes of the prepared samples were significantly affected by the reaction conditions (hydrothermal treatment time, organic additive, pH value and the amount of EDTA in the synthesis solution). The characteristic emission of the spherical $YP_xV_{1-x}O_4:Ln^{3+}$ (Ln = Eu, Sm, Dy or Tm) phosphors were investigated in detail. The results showed that the light color of the $YP_{0.3}V_{0.7}O_4$ microspheres can be easily adjusted by doping different lanthanide activators; $Y_{0.93}Sm_{0.07}P_{0.3}V_{0.7}O_4$ and $Y_{0.95}Eu_{0.05}P_{0.3}V_{0.7}O_4$ exhibited strong orange-red and red emission, respectively, and $Y_{0.93}Sm_{0.07}P_{0.3}V_{0.7}O_4$ has a higher quantum efficiency of 76.8%. For the $Y_{0.97}Dy_{0.03}P_xV_{1-x}O_4$ (x = 0.3–0.9) samples, both emission intensities of Dy^{3+} and VO_4^{3-} increase with increasing the P amount, and the quantum efficiency of $Y_{0.97}Dy_{0.03}P_{0.9}V_{0.1}O_4$ can reach 92%. It can also be found that the light color of the $Y_{0.97}Dy_{0.03}P_xV_{1-x}O_4$ samples can be tuned by changing the ratio of P/V, and $Y_{0.97}Dy_{0.03}P_{0.5}V_{0.5}O_4$ can emit white light under UV excitation.

1 Introduction

Up to now, many efforts have been devoted to the design and preparation of inorganic nano- or micro-scale crystals with controllable morphologies and accurately tunable sizes in modern materials chemistry, due to the close relationship between the physicochemical properties of inorganic functional materials and their architectures (*e.g.* shape, size, exposed facets and dimensionality, *etc.*).[1] Numerous micro/nanomaterials with different specific morphologies and sizes, including nanowires,[2] nanoplates,[3] nanotriangles,[4] mesoporous structures,[5] microspheres,[6] microflowers[7] *etc.*, have been fabricated by various methods, especially the hydrothermal synthesis method. During the hydrothermal process, organic complex agents (*i.e.*, trisodium citrate (Cit^{3-}),[8] ethylenediaminetetraacetic disodium salt (Na_2EDTA)[9] and polyvinylpyrrolidone (PVP)[10]) are often used to prepare the uniform inorganic compounds with special morphologies. The difference in chelating constant and molecular structure of these organic complex agents might lead to the formation of products with different morphologies and sizes by a change of growth orientation in the phase transformation processes.[11,12]

Rare Earth (RE) compounds have attracted extensive attentions because of their technological applications in high-performance luminescent devices, magnets, catalysts, and other functional materials.[13,14] Among various rare earth compounds, rare earth phosphate and vanadate phosphors have been widely studied and applied as commercial luminescent materials, such as the utilization of the classic green and red phosphors $LaPO_4:Tb^{3+}$ and $YVO_4:Eu^{3+}$ in the cathode ray tubes and fluorescent lamps. The RE vanadates are isostructural as the RE phosphates, and they have monoclinic (monazite) or tetragonal (xenotime/zircon) crystal structures,[15] which stimulates the development of mixed phosphovanadate phosphors with a number of advantageous luminescent properties. For instance, the phosphate–vanadate phosphors are more stable and have better luminescent properties at high temperature.[16] Riwotzki and Haase have investigated the luminescent properties of $YP_{0.95}V_{0.05}O_4$:Eu nanoparticles in detail, and found out that there existed efficient energy transfer processes in $YP_{0.95}V_{0.05}O_4$:Eu nanoparticles.[17] Furthermore, doped different luminescent activators in $YP_xV_{1-x}O_4$, their emission colors can be tuned.[18,19]

As is well-known, Eu^{3+}, Sm^{3+} and Dy^{3+} are good luminescent activators, and $YVO_4:Eu^{3+}$ is a commercial red ($^5D_0 \rightarrow {}^7F_2$ of Eu^{3+} at 619 nm) phosphor and $YVO_4:Sm^{3+}$ yields orange-red emission ascribing to the transitions of $^4G_{5/2} \rightarrow {}^6H_{J/2}$ (J = 5, 7, 9 and 11). The characteristic emissions of Dy^{3+} originate from the typical blue transition ($^4F_{9/2} \rightarrow {}^6H_{15/2}$) and yellow one ($^4F_{9/2} \rightarrow {}^6H_{13/2}$), and the yellow to blue intensity ratio can be adjusted to obtain white light emission for Dy^{3+}-doped luminescent materials. For example, $YP_{0.8}V_{0.2}O_4$:1 at% Dy^{3+} and 0.75 at% Sm^{3+} show the strong white light emission.[20] Besides, as a promising phosphor, the proper morphology and particle size

[a]*Research Institute of Applied Catalysis, Shanghai Institute of Technology, China. E-mail: gzhlu@ecust.edu.cn; jerryxiaozh@163.com*

[b]*Key Laboratory for Advanced Materials and Research Institute of Industrial Catalysis, East China University of Science and Technology, China*

are very important to improve their luminescent properties. The optimum morphology is spherical and assembled spheres with a narrow size distribution, and can provide another opportunity to achieve emission tailoring to significantly improve the optical performance, because of the high packing density and reduced light scattering of these spheres.[21] To the best of our knowledge, up till now there is no report on the preparation of the rare earth ions doped assembled spheres $YP_xV_{1-x}O_4$ phosphors, which can achieve tunable colors with higher quantum efficiency as well as white light emission.

Herein, we report a mild complexing-agent assisted hydrothermal process to prepare $YP_xV_{1-x}O_4$ assembled spheres and $YP_xV_{1-x}O_4$:Ln^{3+} (Ln = Eu, Sm, Dy or Tm) phosphors with high quantum efficiency. Trisodium citrate (Cit^{3-}), ethylenediaminetetraacetic acid (EDTA), ammonium oxalate (AO), polyvinylpyrrolidone (PVP) and malonic acid (MA) were chosen as complex agents to manipulate the morphology and particle size of the prepared materials. The effect of the synthesis conditions, such as the synthesis time, organic additive, pH value and added EDTA amount of the synthesis solution, on the structures and shapes of the prepared materials were investigated in detail. Based on the experiment results, the possible crystalline growth mechanism of the $YP_xV_{1-x}O_4$ microspheres was discussed. Finally, we concentrated on the luminescence properties of $YP_{0.3}V_{0.7}O_4$ microsphere-doped with different Ln^{3+} (Ln = Eu, Sm, Dy and Tm) ions. The effect of P/V on the emission colors, the intensity of Dy-doped $YP_xV_{1-x}O_4$ and the effect of Ln loading on the emission intensity of spherical $YP_{0.3}V_{0.7}O_4$:Ln^{3+} (Ln = Eu, Sm and Dy) phosphors were studied, and the materials which can emit the white light under UV excitation have been obtained.

2 Experimental

2.1 Chemicals and materials

All the chemicals were purchased from Shanghai Chemical Reagents Co. and used without further purification.

Ln_2O_3 (Eu_2O_3, Sm_2O_3, Dy_2O_3 and Tm_2O_3) was dissolved into concentrated nitric acid, the excessive nitric acid was evaporated by heating, and then deionized water was added to form the 0.05 M Ln $(NO_3)_3$ solution.

$Y_{0.95}Eu_{0.05}P_{0.3}V_{0.7}O_4$ phosphor was prepared as follows. 1.448 g EDTA was dissolved in 20 mL deionized water, then 1 mL 0.05 M $Eu(NO_3)_3$ and 4.75 mL 0.2 M $Y(NO_3)_3$ were added into the above solution. After vigorous stirring for 30 min, Ln^{3+}–EDTA (Ln = Y and Eu) complex solution (1) was obtained. Subsequently, 1.4 mmol NH_4VO_3 was dissolved in 2 mL concentrated nitrate acid under stirring, and then 0.6 mmol $(NH_4)_2HPO_4$ was added to obtain the mixed solution (2) of NH_4VO_3 and nitrate acid. After stirring for 30 min, the Ln^{3+}–EDTA (Ln = Y and Eu) mixed solution (1) was added dropwise into the solution (2) under stirring. The pH value of this synthesis solution was adjusted by adding ammonia. After stirring for 3 h, the synthesis solution was transferred into a 100 mL Teflon-lined stainless steel autoclave. The autoclave was sealed and maintained at 180 °C for 24 h, and then cooled to room temperature in air. The solid product formed was collected by centrifugation, washed with deionized water and absolute alcohol several times, and finally dried at 80 °C in air for further characterization.

Additionally, other organic additives, including ammonium oxalate (AO), polyvinylpyrrolidone (PVP), trisodium citrate (Cit^{3-}) and malonic acid (MA) were also used to prepare $YP_{0.3}V_{0.7}O_4$ luminescent material (the organic additive/Y^{3+} of 2/1, and pH of 0.57), respectively. All the other samples were prepared using the required stoichiometric amounts under the same conditions. The similar processes were employed to prepare $Y_{1-y}Ln_yP_{0.3}V_{0.7}O_4$ (Ln = Eu^{3+}, Sm^{3+} and Tm^{3+}; y = 0.01, 0.03, 0.05, 0.07, 0.09) and $Y_{0.97}Dy_{0.03}P_xV_{1-x}O_4$ (x = 0.3, 0.5, 0.7, 0.9) samples.

2.2 Characterization of samples

The X-ray diffraction (XRD) patterns of the samples were collected on a PANalytical X' Pert PRO X-ray diffractometer with CuKα radiation (λ = 1.5405 nm; 40 kV, 40 mA). Scanning electron microscopy (SEM) images of the samples were taken on a Hitachi S-3400N scanning electron microscope. The photoluminescence (PL) excitation and emission spectra were recorded on a Hitachi F-4600 fluorescence spectrophotometer equipped with a 150 W xenon lamp as the excitation source. The luminescence life times (τ) were examined on an Edinburgh FLS920 phosphorimeter. The quantum yield can be defined as the integrated intensity of the luminescence signal divided by the integrated intensity of the absorption signal. The absorption intensity was calculated by subtracting the integrated intensity of the light source with the sample from the integrated intensity of the light source with a blank sample in the integrating sphere. All the measurements were performed at room temperature.

3 Results and discussion

3.1 The XRD patterns of as-prepared samples

The XRD patterns of YVO_4, YPO_4 and $YP_xV_{1-x}O_4$ (x = 0.3–0.9) samples were given in Fig. 1. All the diffraction peaks of prepared YVO_4 are in good agreement with the tetragonal YVO_4 (JCPDS 17-0341), and all the peaks of YPO_4 can be indexed to the tetragonal YPO_4 (JCPDS 11-0254). YVO_4 and YPO_4 exhibit the similar XRD patterns except for slight shift of diffraction peaks, because they have the same crystal structure with similar lattice constants (a = 7.1183 Å and c = 6.2893 Å for YVO_4; a = 6.8817 Å and c = 6.0177 Å for YPO_4), which favors the formation of single phase $YP_xV_{1-x}O_4$. All the diffraction peaks of $YP_xV_{1-x}O_4$ are similar to those of the tetragonal YVO_4 and YPO_4, and their corresponding XRD peaks shift gradually between those of the YVO_4 and YPO_4. As shown in the inset of Fig. 1, the diffraction peak (200) at $2\theta = 25.8°$ for the $YP_{0.7}V_{0.3}O_4$ consists of a single peak rather than two respective peaks of YVO_4 and YPO_4, which is also found in other $YP_xV_{1-x}O_4$ (x = 0.3, 0.5, 0.9) samples. Furthermore, the lattice constants of $YP_xV_{1-x}O_4$ (x = 0.3, 0.5, 0.7, 0.9) are calculated by $l/d_{hkl}{}^2 = (h^2 + k^2)/a^2 + l^2/c^2$, where d_{hkl} is the Bragg diffraction spacing for the (h k l) facets and h, k, l are miller indices, a and c are cell parameters. And the results are

shown in Table 1. It can be found that the lattice constants of samples decreased with an increase in the P amount, which may attribute to the smaller radius of P^{5+} compared with V^{5+}. These results further prove that $YP_xV_{1-x}O_4$ ($x = 0.3, 0.5, 0.7, 0.9$) solid solutions with single phase can be obtained by the EDTA-assisted hydrothermal method.

We selected $Y(P,V)O_4$ (P/V = 3/7) as the model sample to investigate the influence of pH value of the solution on its microstructure. The XRD patterns of $Y(P,V)O_4$ (P/V = 3/7) samples prepared at 180 °C for 24 h with the synthesis solution ($EDTA/Y^{3+} = 2/1$, mol) at different pH values (0.23, 0.57, 1, 4, 7 and 10) were shown in Fig. 2. When the pH value was 0.23, the diffraction peaks of sample belong to the tetragonal phase of YPO_4 (JCPDS 11-0254) and the tetragonal YVO_4 was not observed; as pH was 0.57 or 1, the samples exhibited mainly the tetragonal phase of YVO_4 (JCPDS 17-0341), which indicated the successful formation of tetragonal phase of $YP_{0.3}V_{0.7}O_4$. For the sample prepared at pH 4, the mixture phases were observed in the XRD pattern, which belongs to the hexagonal phase $YPO_4 \cdot 0.8H_2O$ (JCPDS 42-0082) and tetragonal phase YVO_4, respectively. For the sample prepared at pH = 7 or 10, the samples are indexed to the hexagonal phase of $YPO_4 \cdot 0.8H_2O$, and tetragonal phase YVO_4 cannot be observed.

The results showed that the optimum pH values range from 0.57 to 1, in which condition the tetragonal phase of $YP_{0.3}V_{0.7}O_4$ can be successfully prepared by the hydrothermal method in the presence of EDTA. Note that the diffraction peaks of samples prepared at pH of 0.57–1 were broadened obviously, possibly due to the small size of the crystallites, which can be seen by SEM pictures.

3.2 The effects of synthesis conditions on the morphology of prepared samples

3.2.1 Effect of PO_4^{3-} on the morphology of $YP_xV_{1-x}O_4$. The morphologies of $YP_xV_{1-x}O_4$ ($x = 0.3, 0.5, 0.7, 0.9$) prepared hydrothermally at 180 °C for 24 h with the synthesis solution ($EDTA/Y^{3+} = 2/1$, mol) at pH 0.57. As shown in Fig. 3, the $YP_xV_{1-x}O_4$ ($x = 0.3, 0.5, 0.7, 0.9$) samples show spherical shape that

Table 1 Lattice constants of the $YP_xV_{1-x}O_4$ phosphors

P/V	3/7	5/5	7/3	9/1
a (Å)	7.1134	7.008	6.9216	6.9118
c (Å)	6.2880	6.1494	6.0403	6.0387

are assembled by numerous smaller particles. With the variation of molar ratio of P/V, the particle size and surface stripe of the sample prepared are obviously different. Comparing with the morphologies of four samples, we selected $YP_{0.3}V_{0.7}O_4$ (P/V = 3/7) as the model sample to study the effect of the synthesis condition (*i.e.* pH value, the molar ratio of $EDTA/Y^{3+}$, organic additives and the synthesis time) on its microstructure and morphology.

3.2.2 Effect of pH value on the morphology of $YP_{0.3}V_{0.7}O_4$. The SEM images of samples prepared at different pH values (0.23, 0.57, 1, 4, 7 and 10) were shown in Fig. 4. The other synthesis conditions were kept unchanged: $EDTA/Y^{3+} = 2/1$ (mol), the synthesis temperature and time were 180 °C and 24 h. When the pH value of the synthesis solution was 0.23, the prepared sample was tetragonal phase YPO_4 (Fig. 1a) with large-scale microsheets-assembled architecture (Fig. 4a). This is because when the pH value is too low, V^{5+} could be reduced to V^{4+}, thus the precipitates of YVO_4 could not form.[22] When the pH value reached 0.57 or 1, the prepared samples belonged to tetragonal $YP_{0.3}V_{0.7}O_4$ (Fig. 1b and c), and they showed sphere-like morphology (Fig. 4b and c). The overall hydrothermal reaction for the tetragonal $YP_{0.3}V_{0.7}O_4$ can be described as follows:

$$V_{10}O_{28}^{6-} + Y^{3+} + PO_4^{3-} + EDTA^{2-} \rightarrow YP_{0.3}V_{0.7}O_4 \text{ (tetragonal phase)}$$

When the pH value of the solution increased to 4, 7 and 10, the morphologies of obtained samples were quite different from the sample synthesized at pH = 1 or 0.57, and exhibited the

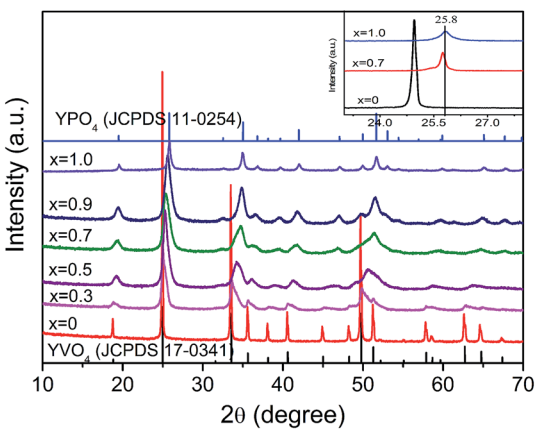

Fig. 1 XRD patterns of $YP_xV_{1-x}O_4$ ($x = 0, 0.3, 0.5, 0.7, 0.9, 1.0$) at pH = 0.57.

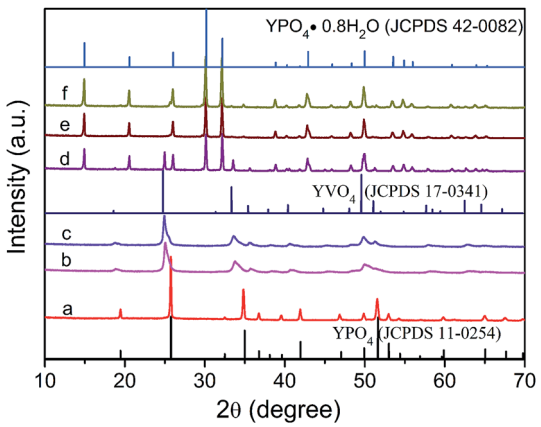

Fig. 2 XRD patterns of samples prepared at pH of (a) 0.23, (b) 0.57, (c) 1, (d) 4, (e) 7 and (f) 10. All samples ($EDTA/Y^{3+} = 2/1$, mol) were hydrothermally synthesized at 180 °C for 24 h.

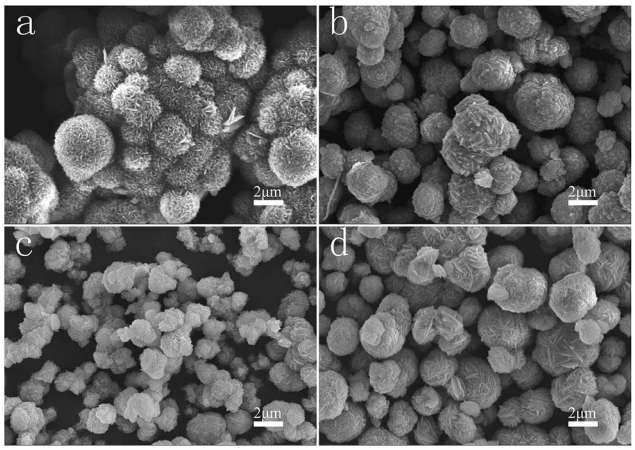

Fig. 3 SEM images of $YP_xV_{1-x}O_4$ at x = (a) 0.3, (b) 0.5, (c) 0.7 and (d) 0.9. All samples were hydrothermally synthesized at 180 °C for 24 h with the synthesis solution (EDTA/Y^{3+} = 2/1, mol) at pH of 0.57.

flower-like structures composed of prism-like microrods (Fig. 4d–f). These kinds of morphologies were similar to the results repeated by Lin *et al.*, and they used trisodium citrate (Cit^{3-}) as additive to fabricate hexagonal prism-like nanoparticles.[18] It is possible when the pH value is higher than 4, hexagonal phase of YPO_4 could easily form and be stable in the solution containing EDTA, resulting in no formation of the tetragonal phase $Y(P,V)O_4$. The results above show that the pH value of the synthesis solution strongly affects the microstructure of the prepared samples, and the appropriate pH value for the preparation of single tetragonal phase $YP_{0.3}V_{0.7}O_4$ with sphere-like morphology are 0.57–1.

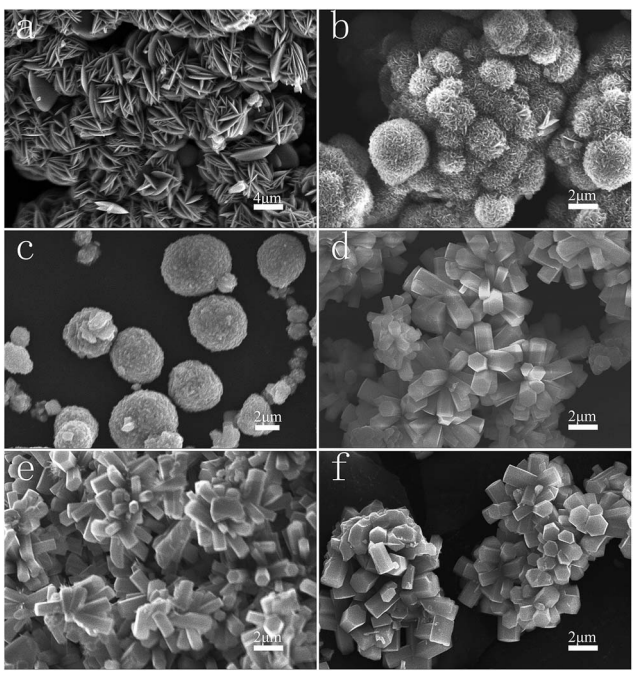

Fig. 4 SEM images of $Y(P,V)O_4$ (P/V = 3/7) samples prepared at pH of (a) 0.23, (b) 0.57, (c) 1, (d) 4, (e) 7 and (f) 10. All samples were hydrothermally synthesized at 180 °C for 24 h with the synthesis solution (EDTA/Y^{3+} = 2/1, mol).

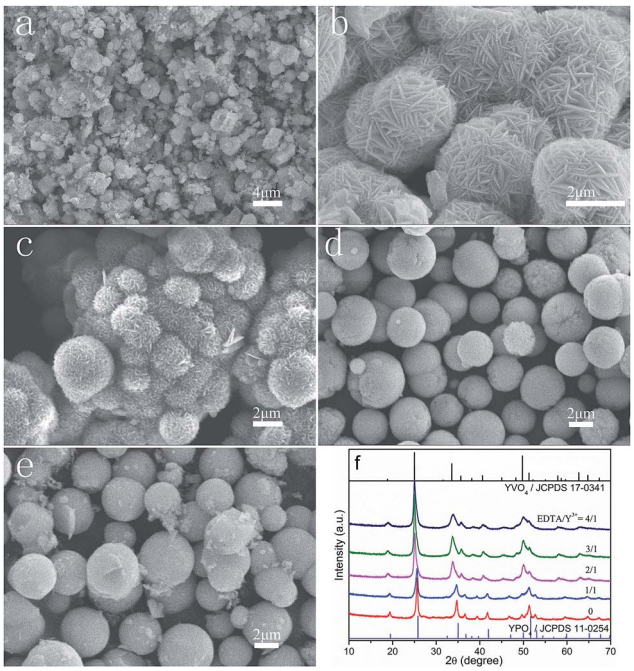

Fig. 5 (a–e) SEM images and (f) XRD patterns of $YP_{0.3}V_{0.7}O_4$ samples prepared at EDTA/Y^{3+} of (a) 0, (b) 1/1, (c) 2/1, (d) 3/1 and (e) 4/1. All samples were hydrothermally synthesized at 180 °C for 24 h and pH = 0.57 of the synthesis solution.

3.2.3 Effect of EDTA amount on the morphology of $YP_{0.3}V_{0.7}O_4$. In the synthesis of inorganic nano/microcrystals, the organic additives could be employed to modify certain crystallographic surfaces of samples.[23] Herein, we adopted the EDTA-assisted method to hydrothermally synthesize the $YP_xV_{1-x}O_4$ samples, and the influence of EDTA amount on the morphologies and the particle sizes of $YP_{0.3}V_{0.7}O_4$ were

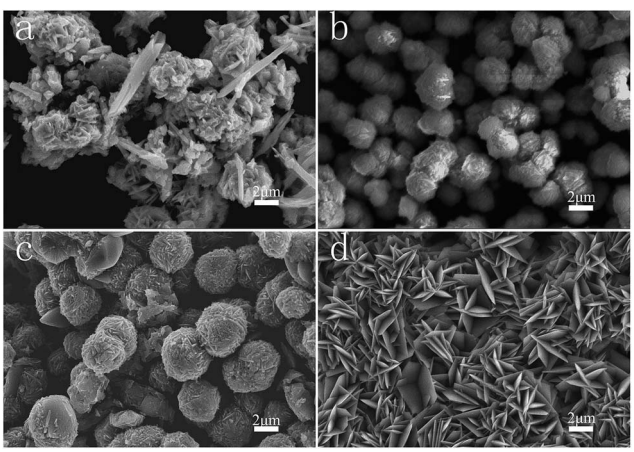

Fig. 6 SEM images of the $YP_{0.3}V_{0.7}O_4$ samples prepared in the presence of (a) AO, (b) PVP, (c) Cit^{3-} and (d) MA. All samples were hydrothermally prepared at 180 °C for 24 h in the synthesis solution (the organic additive/Y^{3+} of 2/1, and pH of 0.57).

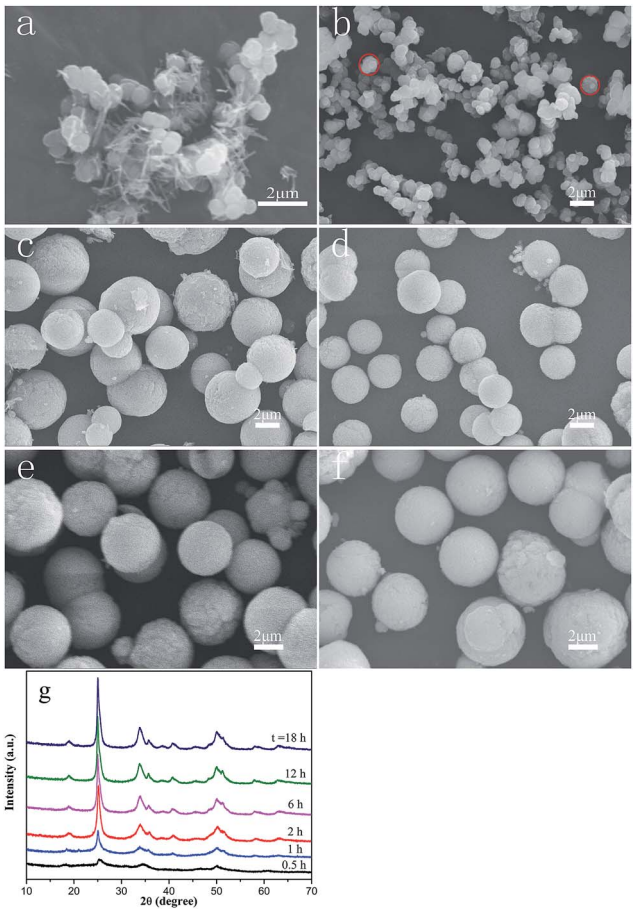

Fig. 7 (a–f) SEM images and (g) XRD patterns of the $YP_{0.3}V_{0.7}O_4$ samples synthesized at 180 °C for (a) 0.5 h, (b) 1 h, (c) 2 h, (d) 6 h, (e) 12 h, (f) 18 h with the synthesis solution (EDTA/Y^{3+} of 3/1, and pH of 0.57).

investigated. The results show that with the increase in the EDTA amount, the diffraction peaks of the sample shifted to lower angles (Fig. 5f), which indicates that the as-prepared samples remain the tetragonal phase $YP_{0.3}V_{0.7}O_4$. However, the morphologies of the samples have a drastic change. As shown in Fig. 5a, without adding EDTA, the sample was only composed of numerous irregular aggregated microparticles with a broad size distribution. When the molar ratio of EDTA/Y^{3+} was controlled to 1 : 1 or 2 : 1, as-prepared $YP_{0.3}V_{0.7}O$ samples present quasi-sphere microparticles with numerous nanosheets or pine needle-like (Fig. 5b and c). Further increasing the EDTA/Y^{3+} molar ratio to 3/1 or 4/1, the obtained samples still remain the sphere-like morphology with smooth surface (Fig. 5d and e). The above results show that EDTA added in the synthesis solution plays an important role on the formation of $Y(P,V)O_4$ with sphere-like morphologies.

In addition, other organic additives, such as ammonium oxalate (AO), polyvinylpyrrolidone (PVP), trisodium citrate (Cit^{3-}) and malonic acid (MA) were also used to test their effects on the morphologies of prepared samples. With the synthesis solution (the organic additive/Y^{3+} of 2/1, and pH of 0.57), the $YP_{0.3}V_{0.7}O_4$ samples were prepared hydrothermally at 180 °C for 24 h. The SEM images of the $YP_{0.3}V_{0.7}O_4$ samples prepared with different organic additives (AO, PVP, Cit^{3-} and MA) are given in Fig. 6. As shown, when the AO was used as organic additive, the prepared sample exhibited mainly irregular nanosized flower-like particles (Fig. 6a); using the PVP or Cit^{3-} additive, the samples showed the sphere-like microparticles with some crystal ridges (Fig. 6b and c); as malonic acid was employed as an organic additive, the obtained sample was almost entirely monodispersed microflowers composed of numerous blades (Fig. 6d).

As shown in the above results, when the PVP, EDTA and Cit^{3-} were employed as the organic additives, the prepared samples present the similar sphere-like morphologies. This is because that PVP, EDTA and Cit^{3-} are excellent chelating agents that can slow down the nucleation rate, and change the shape of the final products.[24]

3.2.4 Effect of synthesis time on the morphology of $YP_{0.3}V_{0.7}O_4$. The influence of the hydrothermal treatment time on the morphology of $YP_{0.3}V_{0.7}O_4$ sample was investigated, and SEM images and XRD patterns of samples are shown in Fig. 7. As shown in Fig. 7a, for the sample prepared for 0.5 h some

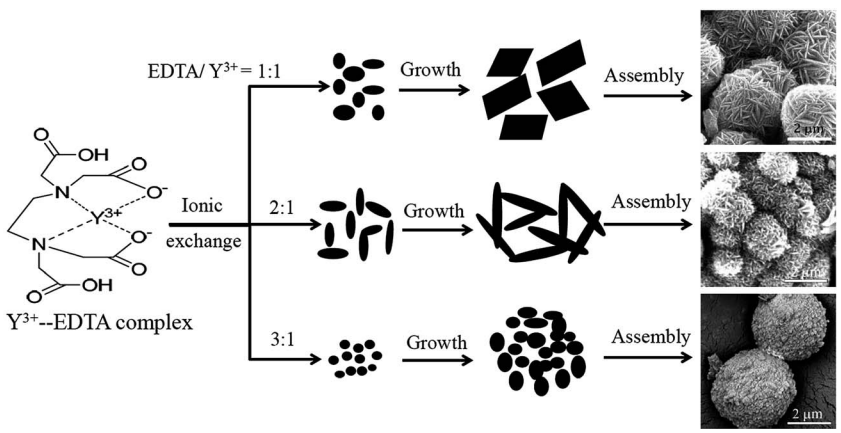

Scheme 1 Schematic illustration for the possible formation mechanism of $Y(P,V)O_4$ with various morphologies under different synthesis conditions.

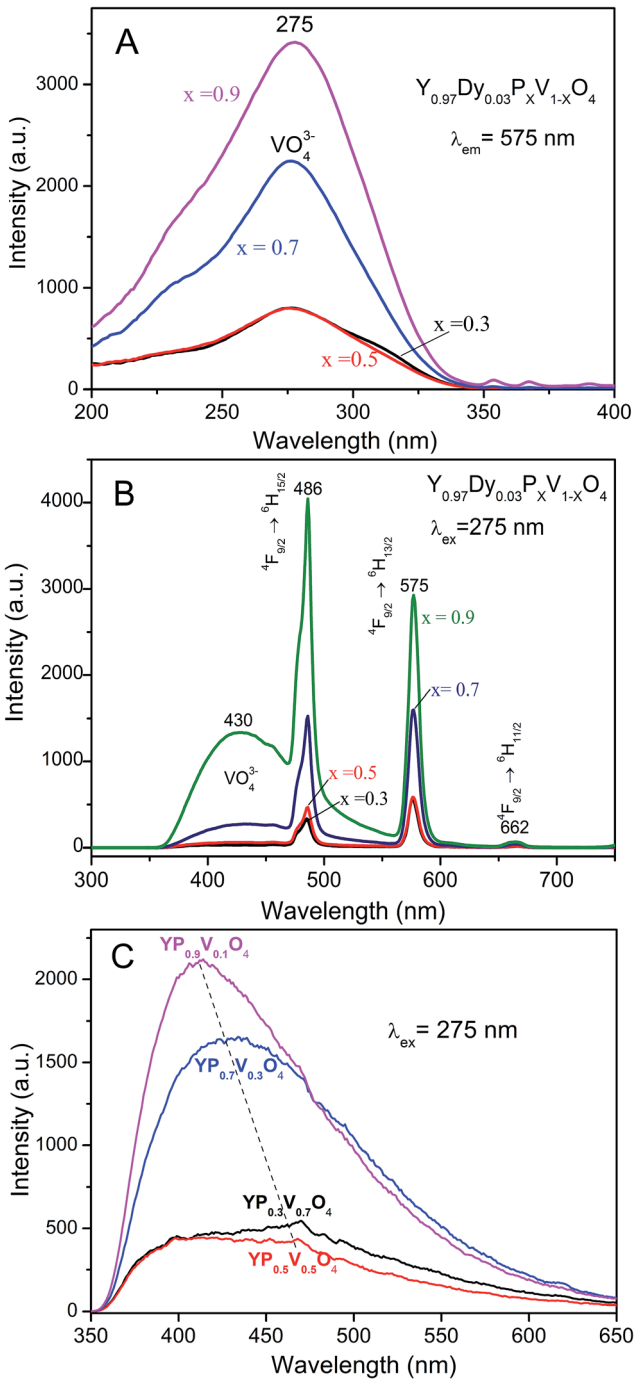

Fig. 8 Excitation (A) and emission (B) spectra of the $Y_{0.97}Dy_{0.03}P_x$-$V_{1-x}O_4$ (x = 0.3, 0.5, 0.7, 0.9) samples, (C) emission spectra of YP_x-$V_{1-x}O_4$ (x = 0.3, 0.5, 0.7, 0.9).

sheets have been formed. As the synthesis time prolonged to 1 h, more sheets were obtained and aggregated together to form quasi-sphere microstructures, which acted as the bases for the subsequent development of microsphere (Fig. 7b). With further increase of hydrothermal treatment time to 2 h, microspheres with irregular size were observed (Fig. 7c), indicating that monosphere 3D $YP_{0.3}V_{0.7}O_4$ phosphors were soon fabricated by this EDTA-assisted hydrothermal method, in which EDTA/Y^{3+} of 3, pH of 0.57 and the reaction temperature of 180 °C were used. Further increasing the synthesis time from 2 to 18 h, the size of formed samples gradually became uniform and were about 2–4 μm, and their crystallines were also improved somewhat (Fig. 7c–f). After this synthesis solution was kept at 180 °C for 18 h, the uniform and monodisperse sphere particles (~4 μm) have been successfully prepared.

3.3 The formation mechanism of Y(P,V)O_4

In the solution-phase synthesis, as surfactants or capping agents the organic additives can tune the surface free energies of different facets by their interaction with metal surface, which may significantly affect the relative growth rates of different facets.[23] Lin *et al.* used Cit^{3-} as the organic additive to prepare spherical YVO_4 and also discussed the role of Cit^{3-} on controlling the shape of YVO_4 in detail.[8] Herein, EDTA also plays an important role on promoting the growth of assembled spheres Y(P,V)O_4. In the synthetic process, EDTA can form the intermediate Y^{3+}–EDTA complexes with Y^{3+} ions by stronger coordination interaction, which can control the concentration of free Y^{3+} ions and thus help control the nucleation and growth of the crystals in the view of the dynamic process.[8] Then under the hydrothermal conditions (high temperature and pressure), the chelating of Ln^{3+}–EDTA complexes was attacked by $(P,V)O_4^{3-}$ and an anion-exchange reaction between $(P,V)O_4^{3-}$ and EDTA took place to form Y(P,V)O_4 nuclei. During the subsequent crystal growth stage, the released EDTA may selectively bind to certain specific crystallographic facets. Such the preferential adsorption can effectively restrict or promote the growth along specific directions, resulting in the formation of 2D microsheets. As the EDTA/Y^{3+} molar ratio could be adjusted in the synthesis solution, the growth environment of crystals could be controlled, thus the selective adsorption of EDTA on the different facets on the grew Y(P,V)O_4 nuclei would results in the wealth of shapes of structures, such as, nanorods and nanoparticles. And then microsheets/nanorods/nanoparticles were finally self-assembled to 3D hierarchical spheres, as shown in Scheme 1. All in all, with the increase of EDTA content, the growth of crystalline has been restricted, resulting in the decrease of the particle size of the crystals which are finally assembled into the 3D microspheres. Besides, the self-assembly would also be influenced by other factors, such as crystal face attraction, electrostatic and dipolar fields associated with the aggregate, van der Waals forces, hydrophobic interactions, hydrogen bonds and so on, which make the prepared products showing multiform morphologies.[8]

3.4 Photoluminescence properties of $Y_{0.97}Dy_{0.03}P_xV_{1-x}O_4$ microarchitecture

The emission and excitation spectra of $Y_{0.97}Dy_{0.03}P_xV_{1-x}O_4$ were measured at the room temperature. In the excitation spectra of $Y_{0.97}Dy_{0.03}P_xV_{1-x}O_4$ at the emission wavelength of 575 nm (Fig. 8A), there was a strong absorption at 275 nm due to the charge transfer from the oxygen ligands to the central vanadium atom inside the VO_4^{3-} group, and some weak lines in the longer

wavelength region due to the f–f transitions of Dy^{3+} with its $4f^9$ configuration. Under excitation at 275 nm, the emission spectra of $Y_{0.97}Dy_{0.03}P_xV_{1-x}O_4$ were obtained. As shown in Fig. 8B, a broad emission band at 430 nm was corresponding to the VO_4^{3-} emission, and its emission intensity increased with an increase in the P content, possibly due to the reduction in the non-radiative energy transfer to lanthanide ions. It was reported, when the V lattice sites were replaced by P in the crystal, the separation between –V–V– was increased, resulting in the reduce for the energy transfer to the randomly distributed activators and the enhancement of the radiative recombination within VO_4^{3-}.[19] Besides, the shark peaks are the characteristic emission of Dy^{3+}, ascribing to f–f transition, the magnetic dipole transition ($^4F_{9/2} \rightarrow {}^6H_{15/2}$) at 486 nm and the hypersensitive electric dipole transition ($^4F_{9/2} \rightarrow {}^6H_{13/2}$) at 575 nm. A weak emission band located at 662 nm could also be observed, attributing to the transition of $^4F_{9/2} \rightarrow {}^6H_{11/2}$ of Dy^{3+}. Note that with the increase of the P amount, the emission intensity of Dy^{3+} increased too. As shown in Fig. 8, the $Y_{0.97}Dy_{0.03}P_{0.9}V_{0.1}O_4$ sample exhibited the strongest emission intensity of Dy^{3+} and VO_4^{3-}.

To understand the role of $YP_xV_{1-x}O_4$ host emission on the emission spectra of $Y_{0.97}Dy_{0.03}P_xV_{1-x}O_4$, the emission spectra of $YP_xV_{1-x}O_4$ host under the excitation wavelength of 275 nm were measured and shown in Fig. 8C. It can be found that a broad emission peak at 430 nm appeared from the emission of VO_4^{3-} group, and the emission intensity of VO_4^{3-} were varied with the P content, which was agreement with that of $Y_{0.97}Dy_{0.03}P_xV_{1-x}O_4$. Note that the emission intensity of VO_4^{3-} group in $Y_{0.97}Dy_{0.03}P_xV_{1-x}O_4$ was lower than that of $YP_xV_{1-x}O_4$ without the Dy^{3+} dopant, indicating that there exists an efficient energy transfer between VO_4^{3-} and Dy^{3+}. The excitation and emission processes of VO_4^{3-} and the energy transfer and emission processes of Ln^{3+} ions are schematically shown in Fig. 9, which is similar to that reported.[8] In the $Y_{1-y}Ln_yP_xV_{1-x}O_4$ phosphors, as the excitation energy cannot be transferred by PO_4^{3-} groups, and VO_4^{3-} groups can act as a bridge between the host absorption and the Ln^{3+} luminescent center. Under UV excitation, the energy transfer process can be described as follows: firstly, the UV radiation was adsorbed by VO_4^{3-} group, and then part of energy was transferred to Ln^{3+} luminescence center after a thermally activated energy migration through the vanadate sublattice, finally relaxed as the characteristic emissions of Ln^{3+}. Part of energy may be relaxed directly to the ground state of the VO_4^{3-} groups, producing the broad band emission of VO_4^{3-}. Therefore, we can observe the emission of Ln^{3+} and VO_4^{3-} together in the emission spectra of $Y_{0.97}Dy_{0.03}P_{0.9}V_{0.1}O_4$ and $Y_{0.97}Dy_{0.03}P_{0.7}V_{0.3}O_4$, respectively.

The quantum yield of $Y_{0.97}Dy_{0.03}P_{0.9}V_{0.1}O_4$ sample was measured to be 92%, which is higher than that reported. For example, the quantum yield of YVO_4: 5 mol%Dy^{3+} prepared in the presence of Cit^{3-} was 62%,[8] and the quantum efficiency of $YP_{0.8}V_{0.2}O_4$: 1 at% Dy^{3+}-0.75 at% Sm^{3+} was 25%.[20] In order to better understand the influence of the P content on the color of light emission for these samples, the CIE coordinates of these samples were calculated on the basis of the luminescence spectra and listed in Table 2. It can be found that, with an increase in the P content, the coordinate positions gradually shifted towards blue color position. When the molar ratio of P/V is 0.5/0.5, $Y_{0.97}Dy_{0.03}P_{0.5}V_{0.5}O_4$ sample has generated white light

Table 2 CIE chromaticity coordinates of the $Y_{0.97}Dy_{0.03}P_xV_{1-x}O_4$ (x = 0.3, 0.5, 0.7, 0.9) samples

Sample (x value)	Excitation (nm)	CIE chromaticity coordinate		Emission color
		X	Y	
0.3	275	0.34	0.37	White
0.5	275	0.31	0.33	White
0.7	275	0.28	0.29	Bluish white
0.9	275	0.23	0.22	Blue

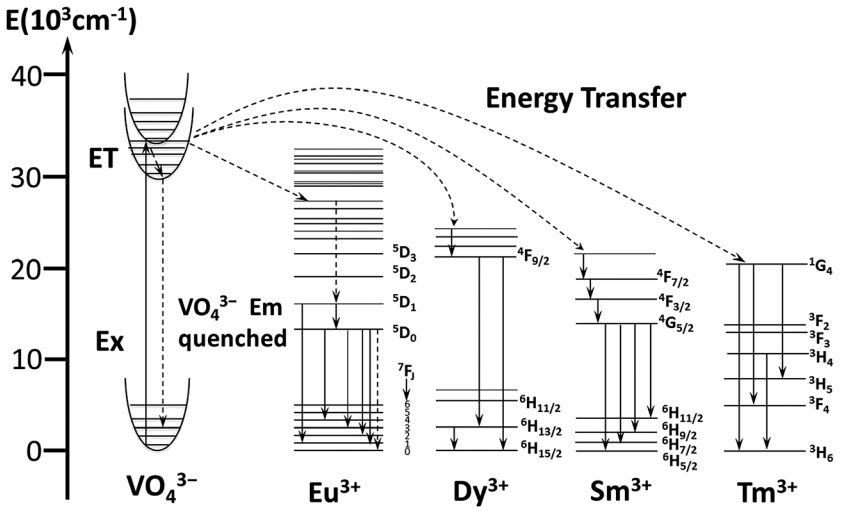

Fig. 9 The proposed energy transfer processes in $Y(P,V)O_4:Ln^{3+}$ (Ln = Eu, Sm, Dy, Tm) samples.

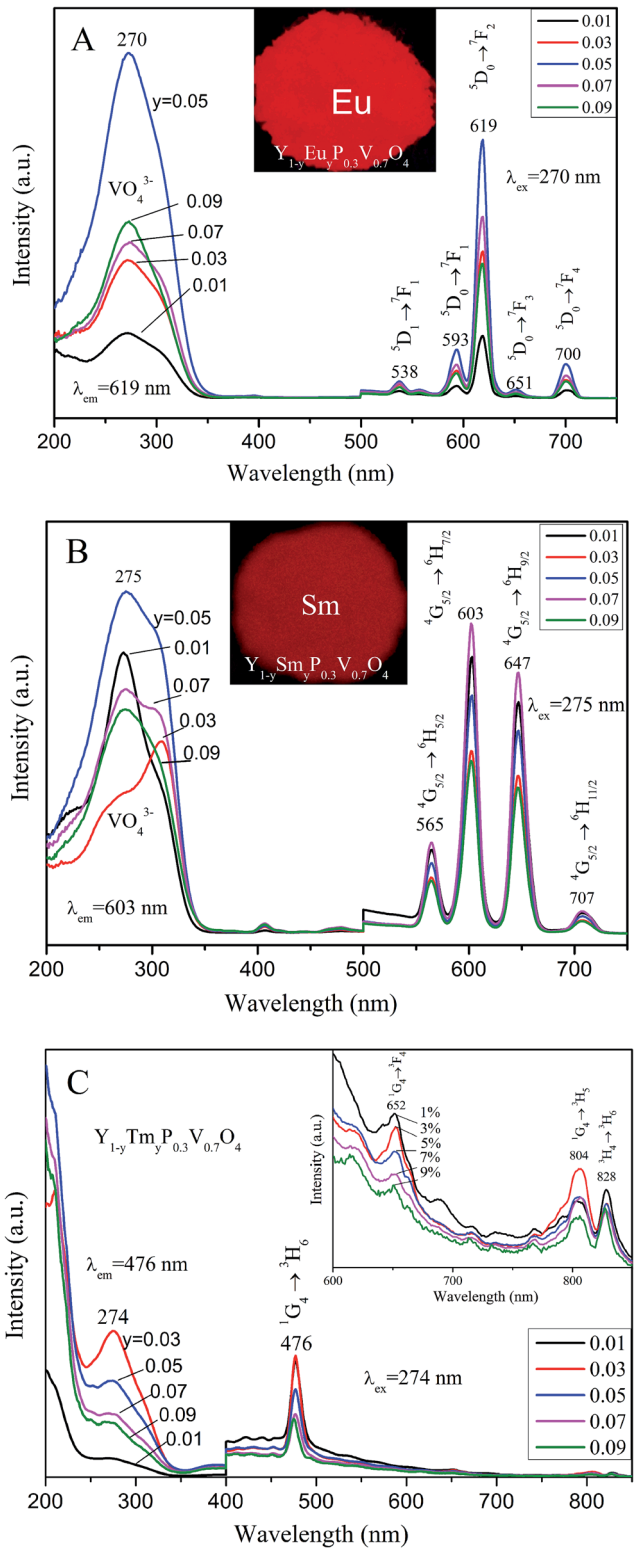

Fig. 10 Excitation and emission spectra for $Y_{1-y}Ln_yP_{0.3}V_{0.7}O_4$ (Ln = (A) Eu, (B) Sm and (C) Tm; y = (0.01, 0.03, 0.05, 0.07 and 0.09)). Insets are the direct view photos when being excited at 254 nm.

emission with the CIE (Commission International de I'Eclairage) chromaticity coordinate of (0.31, 0.33), which is close to ideal white light (0.33, 0.33).

3.5 Photoluminescence properties of Ln-doped $YP_{0.3}V_{0.7}O_4$ samples

We used $YP_{0.3}V_{0.7}O_4$ as a host and doped with Ln-luminescent activators to adjust the color of light emission. Fig. 10 shows the room-temperature excitation and emission spectra of the $Y_{1-y}Ln_yP_{0.3}V_{0.7}O_4$ (y = 0.01, 0.03, 0.05, 0.07 and 0.09; Ln = Eu^{3+}, Sm^{3+} and Tm^{3+}) samples. In the excitation spectra of the $Y_{1-y}Ln_yP_{0.3}V_{0.7}O_4$ (Ln = Eu^{3+}, Sm^{3+} and Tm^{3+}) samples, the most strongest emission peaks of Eu^{3+}, Sm^{3+} and Tm^{3+} are located at 619, 603 and 476 nm, corresponding to the transitions of $^5D_0 \rightarrow {}^7F_2$ from Eu^{3+}, $^4G_{5/2} \rightarrow {}^6H_{7/2}$ from Sm^{3+}, $^1G_4 \rightarrow {}^3H_6$ of Tm^{3+} respectively, and a strong and broad band at 270–275 nm is ascribed to the charge transfer within the VO_4^{3-} groups, which confirms that the emission of Ln^{3+} produced by an energy transfers from the excited VO_4^{3-}. As their shapes were nearly identical, their peak positions were hardly changed with the y value. While some weak lines can be also observed in the longer wavelength region due to the f–f transitions of Ln^{3+} with its $4f^9$ configuration. Under excitation at 270, 275 and 274 nm, the emission spectra of Eu^{3+}, Sm^{3+} and Tm^{3+}-doped $YP_{0.3}V_{0.7}O_4$ were obtained, respectively (Fig. 10).

In the emission spectra of $Y_{1-y}Eu_yP_{0.3}V_{0.7}O_4$ excited at 270 nm, there were the multiple transitions of $^5D_1 \rightarrow {}^7F_1$ and $^5D_0 \rightarrow {}^7F_J$ (J = 1, 2, 3, 4) of Eu^{3+} ions at 538, 593, 619, 651 and 700 nm, respectively. Among these emission peaks, the red emission at 619 nm from the transition of $^5D_0 \rightarrow {}^7F_2$ was the most prominent and strong. When the Eu^{3+} amount (y) was 5 mol% in $Y_{1-y}Eu_yP_{0.3}V_{0.7}O_4$, the strongest emission spectrum was obtained, and upon excitation at 254 nm with a UV lamp its strong red emission can be seen clearly (inset of Fig. 10A). In general, the Eu^{3+} is an excellent structure probe for investigating the local environment in a host matrix in terms of Judd–Ofelt theory.[25] If the Eu^{3+} ions are located in the sites with an inversion center, the $^5D_0 \rightarrow {}^7F_1$ magnetic dipole transition should be dominant, and in the sites without an inversion center, the $^5D_0 \rightarrow {}^7F_2$ electric dipole transition would be preponderant.[26] As shown in Fig. 10A, the intensity of electric-dipole transitions from $^5D_0 \rightarrow {}^7F_{2,4}$ was much stronger than that of magnetic-dipole transitions from $^5D_0 \rightarrow {}^7F_{1,3}$, which indicates that the Eu^{3+} lattice site is not inversion symmetry. Fig. 10B shows the emission spectra of $Y_{1-y}Sm_y P_{0.3}V_{0.7}O_4$ (y = 0.01–0.09), which exhibits the typical red-orange emissions at 565, 603, 647 and 707 nm ascribing to the transitions from $^4G_{5/2} \rightarrow {}^6H_J$ (J = 5/2, 7/2, 9/2 and 11/2), respectively. When the Sm^{3+} amount (y) was 7 mol% in $Y_{1-y}Sm_yP_{0.3}V_{0.7}O_4$, the strongest PL emission intensity was obtained.

Fig. 10C displays the emission spectra of $Y_{1-y}Tm_yP_{0.3}V_{0.7}O_4$ (y = 0.01–0.09), and a typical blue emission band at 476 nm could be detected, corresponding to the transition of $^1G_4 \rightarrow {}^3H_6$. Other weak bands in infrared region were located at 652, 804 and 828 nm, assigned to the transitions of $^1G_4 \rightarrow {}^3F_4$, $^1G_4 \rightarrow {}^3H_5$ and $^3H_4 \rightarrow {}^3H_6$, respectively[27] (inset of Fig. 9C). When the Tm^{3+} amount (y) was 3 mol% in $Y_{1-y}Tm_yP_{0.3}V_{0.7}O_4$, the strongest PL emission intensity could be obtained.

The above results indicate that an efficient energy transfer also occurred from VO_4^{3-} to Eu^{3+}, Sm^{3+} and Tm^{3+} in Ln-doped

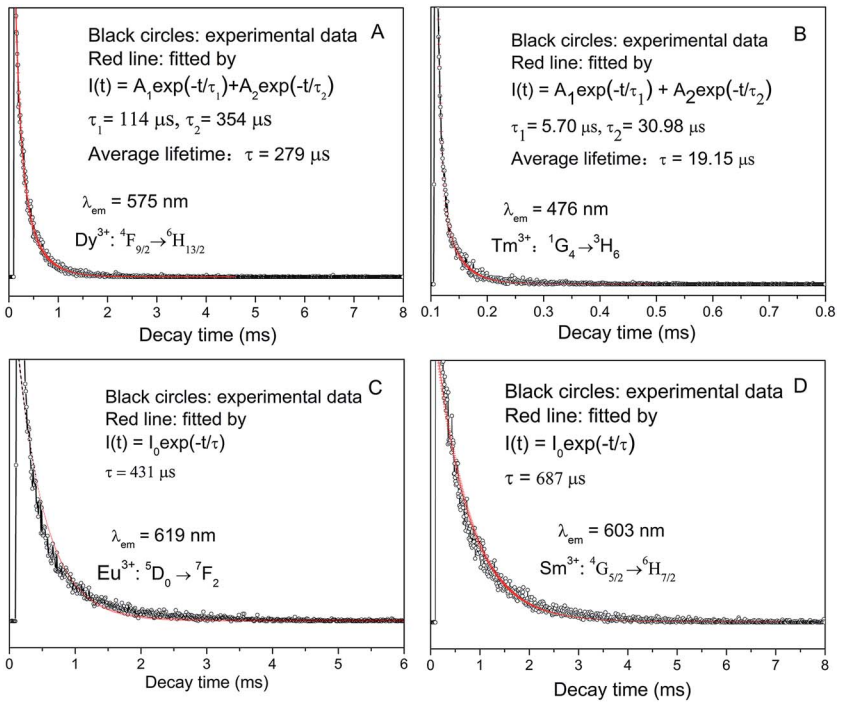

Fig. 11 Decay curves of (A) $Y_{0.97}Dy_{0.03}P_{0.9}V_{0.1}O_4$ and $YP_{0.3}V_{0.7}O_4$:Ln^{3+} (Ln = (B) Tm, (C) Eu, (D) Sm) samples.

$YP_{0.3}V_{0.7}O_4$ samples, respectively. The energy transfer processes for $YP_{0.3}V_{0.7}O_4$:Ln^{3+} (Ln = Eu^{3+}, Sm^{3+}, Tm^{3+}) are similar to that of the $YP_{0.3}V_{0.7}O_4$:Dy^{3+}, and are also presented in Fig. 9. Among these phosphors, the energy transfer between Tm^{3+} and VO_4^{3-} is the lowest efficient, resulting in the weak blue emission of Tm^{3+}. $YP_xV_{1-x}O_4$:Ln^{3+} phosphors can exhibit the efficient and characteristic emission under UV excitation, which is very important for the solid state lighting.

Furthermore, we found that the optimum concentration of Sm^{3+} is higher than that of Eu^{3+} in the spherical Ln-doped $YP_{0.3}V_{0.7}O_4$ sample. In most cases, the optimum concentration of Sm^{3+} is much lower than that of Eu^{3+} in the same host lattice due to the active cross-relaxation process in close Sm^{3+}–Sm^{3+} pairs which will quench the luminescence.[28] Hence, we speculate that the cross-relaxation process in close Sm^{3+}–Sm^{3+} pairs is inactive in the assembled spherical $YP_{0.3}V_{0.7}O_4$ host matrix, so its quenching concentration would be high.

The fact that the emission color of $YP_{0.3}V_{0.7}O_4$ can be tuned by doping different lanthanide activators can be confirmed by the CIE chromaticity coordinates. The chromaticity coordinates of the $YP_{0.3}V_{0.7}O_4$: 5 mol% Eu^{3+} sample are $x = 0.615$ and $y = 0.3792$, and emits red light, which agrees well with the luminescence photograph (inset in Fig. 10A). For the samples doped with Sm (7 mol%) or Tm (3 mol%), its chromaticity coordinates are (0.5864, 0.4094) or (0.2004, 0.22), which represents red-orange or light blue color.

Fig. 11A and B shows the luminescent decay curves of the $Y_{0.97}Dy_{0.03}P_{0.9}V_{0.1}O_4$ and $Y_{0.97}Tm_{0.03}P_{0.3}V_{0.7}O_4$ samples, which can be fitted into a double-exponential function as $I = A_1\exp(-t/\tau_1) + A_2\exp(-t/\tau_2)$, where τ_1 and τ_2 are the fast and slow components of the luminescence lifetimes, and A_1 and A_2 are the fitting parameters, respectively. For Dy^{3+}, two lifetimes, the faster one $\tau_1 = 114$ μs, and the slow one $\tau_2 = 354$ μs, have been obtained for the emission of Dy^{3+} at 575 nm. The average lifetime is defined as $[\tau] = (A_1\tau_1^2 + A_2\tau_2^2)/(A_1\tau_1 + A_2\tau_2)$, which is 279 μs. For Tm^{3+}, two lifetimes, the faster one $\tau_1 = 5.70$ μs, and the slow one $\tau_2 = 30.98$ μs, have been obtained for the emission of Tm^{3+} at 476 nm. The average lifetime for Tm^{3+} was calculated to be 19.15 μs. Recently, the double exponential decay behavior of the activator is frequently observed when the excitation energy is transferred from the donor (matrix) to the activator.[29] This is because that the luminescent centers in these hosts lay in the unhomogeneous environment, which would raise the structure disordering, surface defects and impurities.

As shown in Fig. 11C and D, the luminescence decay curves of both Eu^{3+} (5 mol%) and Sm^{3+} (7 mol%) samples can be fitted into a mono-exponential function as $I = I_0\exp(-t/\tau_1)$. The lifetime for Eu^{3+} or Sm^{3+} in $YP_{0.3}V_{0.7}O_4$ materials are 431 or 687 μs respectively. Among these $Y_{1-y}Ln_yP_{0.3}V_{0.7}O_4$ (Ln = Eu^{3+}, Sm^{3+} and Tm^{3+}) luminescence materials, the $Y_{0.93}Sm_{0.07}P_{0.3}V_{0.7}O_4$ shows the longest life time. Its quantum yield was measured to be 76.8% by using an integrated sphere, which is higher than the value (50%) of YVO_4: 5 mol% Sm^{3+}.[8]

4 Conclusions

In summary, the $YP_xV_{1-x}O_4$ assembled spheres with tetragonal phase were prepared successfully by a simple and mild hydrothermal method, and the microstructures of the samples would vary remarkably with varying reaction conditions, including the reaction time, different organic additives, pH value and the

EDTA amount in the synthesis solution. In the presence of EDTA, tetragonal $YP_{0.3}V_{0.7}O_4$ microsphere can be successfully fabricated at pH 0.57–1 of the synthesis solution.

Under ultraviolet excitation, the characteristic emission of Eu^{3+}, Sm^{3+} and Tm^{3+} can be observed in the luminescent spectra of the spherical $Y_{1-y}Ln_yP_{0.3}V_{0.7}O_4$ phosphors (Ln = Eu, Sm, and Tm). $Y_{0.93}Sm_{0.07}P_{0.3}V_{0.7}O_4$ and $Y_{0.95}Eu_{0.05}P_{0.3}V_{0.7}O_4$ exhibit the strong orange-red and red emission, respectively, which indicates that the light colors of the $YP_{0.3}V_{0.7}O_4$ microspheres can be easily adjusted by doping different lanthanide activators. The studies on the luminescent properties of $Y_{0.97}Dy_{0.03}P_xV_{1-x}O_4$ (x = 0.3–0.9) show that the emission intensities of Dy^{3+} and VO_4^{3-} increase with the increase in the P amount, and the white light can also be obtained in $Y_{0.97}Dy_{0.03}P_{0.5}V_{0.5}O_4$ under UV excitation. The spherical $Y_{0.97}Dy_{0.03}P_{0.9}V_{0.1}O_4$ and $Y_{0.93}Sm_{0.07}P_{0.3}V_{0.7}O_4$ phosphors have possessed the strong emission ability, and their quantum efficiency could reach to 92% and ~77%, respectively. The merits of multicolor emissions and higher quantum efficiency of these Ln-doped $YP_xV_{1-x}O_4$ assembled spheres in the visible region endow this approach and luminescent materials to be an alternative towards the development of pcLED for solid state lighting application.

Acknowledgements

We would like to acknowledge the financial support from the National Basic Research Program of China (2010CB732300).

Notes and references

1 (*a*) A. P. Alivisatos, *Science*, 1996, **271**, 933–937; (*b*) J. Hu, T. W. Odom and C. M. Lieber, *Acc. Chem. Res.*, 1999, **32**, 435–445; (*c*) C. M. Burda, C. R. Narayanan and M. A. El-Sayed, *Chem. Rev.*, 2005, **105**, 1025–1102; (*d*) Z. L. Wang, J. H. Hao and H. L. W. Chan, *J. Mater. Chem.*, 2010, **20**, 3178–3185.
2 C. Mu and J. He, *Mater. Res. Bull.*, 2012, **47**, 491–496.
3 X. C. Jiang, L. D. Sun, W. Feng and C. H. Yan, *Cryst. Growth Des.*, 2004, **4**, 517–520.
4 R. Jin, Y. Cao, C. A. Mirkin, K. L. Kelly, G. C. Schatz and J. G. Zheng, *Science*, 2001, **294**, 1901–1903.
5 Q. L. Luo, S. D. Shen, G. Z. Lu, X. Z. Xiao, D. S. Mao and Y. Q. Wang, *RSC Adv.*, 2012, **2**, 616–621.
6 W. Xu, Y. Wang, X. Bai, B. Dong, Q. Liu, J. S. Chen and H. W. Song, *J. Phys. Chem. C*, 2010, **114**, 14018–14024.
7 J. Yang, C. X. Li, Z. W. Quan, C. M. Zhang, P. P. Yang, Y. Y. Li and J. Lin, *J. Phys. Chem. C*, 2008, **112**, 12777–12785.
8 Z. H. Xu, X. J. Kang, C. X. Li, Z. Y. Hou, C. M. Zhang, D. M. Yang, G. G. Li and J. Lin, *Inorg. Chem.*, 2010, **49**, 6706–6715.
9 L. Xu, X. Y. Yang, Z. Zhai, X. Chao, Z. H. Zhang and W. H. Hou, *CrystEngComm*, 2011, **13**, 4921–4929.
10 G. Jia, C. Zhang, S. Ding, L. Wang, L. Li and H. You, *CrystEngComm*, 2012, **14**, 573–578.
11 L. Xu, J. M. Shen, C. L. Lu, Y. P. Chen and W. H. Hou, *Cryst. Growth Des.*, 2009, **9**, 3129–3136.
12 L. Xu, X. Y. Yang, Z. Zhai, D. X. Gu, H. Pang and W. H. Hou, *CrystEngComm*, 2012, **14**, 7330–7737.
13 J. P. Cotter, J. C. Fitzmaurice and I. P. Parkin, *J. Mater. Chem.*, 1994, **4**, 1603–1609.
14 M. S. Palmer, M. Neurock and M. M. Olken, *J. Am. Chem. Soc.*, 2002, **124**, 8452–8461.
15 L. Niinistö and M. Leskelä, in *Handbook on the Physics and Chemistry of Rare Earths*, ed. K. A. Gschneidner Jr and L. Eyring, Elsevier, Amsterdam, 1987, ch. 59.
16 G. Blasse and B. C. Grabmaier, *Luminescent Materials*, Springer, Berlin, 1994.
17 K. Riwotzki and M. Haase, *J. Phys. Chem. B*, 2001, **105**, 12709–12713.
18 C. Li, Z. Hou, C. Zhang, P. Yang, G. Li, Z. Xu, Y. Fan and J. Lin, *Chem. Mater.*, 2009, **21**, 4598–4607.
19 Z. Y. Hou, P. P. Yang, C. X. Li, L. L. Wang, H. Z. Lian, Z. W. Quan and J. Lin, *Chem. Mater.*, 2008, **20**, 6686–6696.
20 N. S. Singh, N. K. Sahu and D. Bahadur, *J. Mater. Chem. C*, 2014, **2**, 548–555.
21 M. L. Zhao, G. S. Li, J. Zheng, L. P. Li and L. S. Yang, *CrystEngComm*, 2012, **14**, 2062–2070.
22 G. C. Li, K. Chao, H. R. Peng and K. Z. Chen, *J. Phys. Chem. C*, 2008, **112**, 6228–6231.
23 A. R. Tao, S. Habas and P. D. Yang, *Small*, 2008, **4**, 310–325.
24 B. Lim, Y. J. Xiong and Y. N. Xia, *Angew. Chem., Int. Ed.*, 2007, **46**, 9279–9282.
25 (*a*) B. R. Judd, *Phys. Rev.*, 1962, **127**, 750–761; (*b*) G. S. Ofelt, *J. Chem. Phys.*, 1962, **37**, 511–520.
26 G. H. Jia, P. A. Tanner and B. M. Cheng, *Chem. Phys. Lett.*, 2009, **474**, 97–100.
27 H. W. Zhang, X. Y. Fu, S. Y. Niu, G. Q. Sun and Q. Xin, *Solid State Commun.*, 2004, **132**, 527–531.
28 B. Yan and X. Q. Su, *J. Alloys Compd.*, 2007, **431**, 342–347.
29 Z. Q. Li and Y. Zhang, *Angew. Chem., Int. Ed.*, 2006, **45**, 7732–7735.

